AUT Journal of Mechanical Engineering

AUT J. Mech. Eng., 9(1) (2025) 19-32
DOI: 10.22060/ajme.2024.23062.6116

# Design of two layer clamped-clamped microsensor based on classical and non-classical theories

Mohammadreza Davoodi Yekta, Abbas Rahi *

Faculty of Mechanical and Energy Engineering, Shahid Beheshti University, Tehran, Iran

**ABSTRACT:** In this paper, the two-layer micro sensor is modeled as a two-layer clamped-clamped microbeam and it is optimized by using the genetic algorithm. Using the results of this research, clamped-clamped microbeams can be designed in such a way that the performance of microsensors whose structure includes these microbeams will be improved. The quality factor, the sensitivity, and the maximum stress are selected as objective functions. The sensitivity and the quality factor are the functions of the natural frequency. The natural frequency is calculated based on Rayleigh's method. The quality factor is calculated by approximation established on the one layer's quality factor formula. To calculate the maximum stress, the system is assumed as a mass-spring system that has a harmonic displacement and the maximum deflection is the static deflection. The thickness of each layer, the width of the microbeam, and the length of the microbeam are selected as design variables. The optimization is done based on classical and non-classical theory by the genetic algorithm. The results based on both theories are approximately equal. The length of the microbeam is the most important variable and very changes (approximately 190%). The thickness of the silicon layer has the least effect on the results and changes just lower than  (approximately 20%). The results show that when the maximum stress decreases and the sensitivity increases, the quality factor decreases which is undesirable. Maximum sensitivity is obtained when the microbeam is very small.

**Review History:**

Received: May, 27, 2024
Revised: Sep. 14, 2024
Accepted: Nov. 08, 2024
Available Online: Dec. 20, 2024

**Keywords:**

Microsensor
Clamped-Clamped Microbeam
Optimization
Sensitivity
Quality Factor

## 1- Introduction

Micro Electromechanical Systems (MEMS) is one of the most important devices used in many fields. In the last two years, microsensors are noticed because of their ability to detect low-mass particles.

Narita et.al [1] reviewed piezoelectric and magnetostrictive biosensor materials for the detection of viruses. They reported sensitivity and quality factor are the most important functions that describe the accuracy and quality of the sensing. Pachkawade et.al reviewed sensors for the detection and measurement of ultra-fine particles. They investigated micro resonant mass sensors including piezoelectric transducers, piezoelectric mass sensors, and thermally actuated resonant transducers. They also reported some parameters such as the size limit of particles and detection range of the microsensors. Lifshitz et.al [2]calculated thermoelastic damping in micro- and nanomechanical systems. They used Zener's standard model of the linear anelastic solid. They derived the governing equation of the isothermal micro or nanobeams while there is no thermoelastic coupling but there is the modified thermoelastic strain. They could calculate the quality factor for these models of beams. Dennis et.al [3] modeled and simulated the effect of air damping on the frequency and quality factor of Complementary Metal-Oxide Semiconductor (CMOS) MEMS devices and Pan et.al [4] calculated the quality factor of a three-layer Kirchhoff–Love microplate considering three-dimensional heat conduction.

A common model of the MEMS especially microsensors is the microbeam. To calculate different parameters of micro beams, a suitable model is necessary. There are many studies about the modeling of microbeams. Approximately in all of these studies, non-classical theories are used to obtain governing equations. These theories consider the size effect on the strain energy [5-11]. The following is an overview of some of these researches:

Kong et.al [12] calculated the size-dependent natural frequency of the Bernoulli- Euler microbeam. The governing equations are obtained based on the modified couple stress theory and by using Hamilton's principle. Park et.al [13] and Gao et.al [14] investigated Bernoulli-Euler and Timoshenko's microbeam based on the modified couple stress theory respectively.

Rahi [15] analyzed the vibration of multi-layer micro beams based on the modified couple stress theory. The strain

*Corresponding author's email: a_rahi@sbu.ac.ir

and kinetic energy of multi-layer microcantilever beams were obtained while the size effect is considered. The first three frequencies are calculated, and results were validated in the special case that the ratio of material length scale parameter to thickness is zero. Loghman et.al [16] investigated the nonlinear vibration of fractional viscoelastic microbeams. They used the modified couple stress theory and Bernoulli-Euler beam theory to model the microbeam and derive the equations. Also, they modeled viscoelastic material via the fractional Kelvin–Voigt model. Khabaz et.al [17] analyzed the dynamic and vibration of the sandwich microbeam based on the modified strain gradient theory. They modeled the microbeam as a multi-layer microbeam including a piezoelectric layer. Ding et.al [18] analyzed the size-dependent nonlinear dynamic of microbeams by using the modified couple stress theory. Akgoz et.al [19] analyzed microbeams for various boundary conditions based on the strain gradient theory. Littrel et.al [20] modeled cantilever-based piezoelectric microsensors and microactuators. Farokhi et.al [21] investigated the dynamics of imperfect microbeams, Ansari et.al [22] obtained vibration characteristics of piezoelectric microbeams based on the modified couple stress theory, Akgoz et.al [23] modeled shear deformation beam, and Talimian et.al [24] investigated dynamic stability of the size-dependent microbeam.

In recent years, Zhao et.al [25] presented a new Bernoulli–Euler beam model based on modified gradient elasticity, Yin et. al [26] did isogeometric analysis for non-classical Bernoulli-Euler beam model incorporating microstructure and surface energy effects, Esen [27] investigated size-dependent Timoshenko microbeams subjected to a moving load, and Chen [28] et.al reformulated microbeams by incorporating the general strain gradient elasticity theory. Also, some studies modeled microbeams including functionally graded material [29-32].

Kumar et.al [33] analyzed static charge-induced pull-in of an electrostatic MEMS. They proposed the non-linear model and derived closed-form expressions of pull-in voltage for different configurations. Sthuti et.al [34] simulated and analyzed suspension-based single-axis mems capacitive accelerometer. Analytical modeling of the suspensions was presented. Capacitive, displacement, and stress analysis of the accelerometer was done. Based on the results, parallel beam suspension is preferred for higher sensitivity and accuracy whereas Folded beam suspension is preferred for greater structural stability. Pakhare et.al [35] investigated the effects of shear deformation on the static pull-in Instability behavior of narrow rectangular Timoshenko microbeams. They first calculated the results of the maximum beam transverse displacement, for a shear deformable propped-cantilever microbeam under the action of uniformly distributed transverse load, second the finalized six-nodded spectral finite element based on the Timoshenko beam theory was utilized to determine static pull-in instability parameters of narrow microbeams with various fixity conditions and beam thickness to-length ratios. Valizadeh et.al [36] investigated the effects of the material dielectricity on the performance of capacitive microdevices. They demonstrated the ability of dielectric materials to reduce the required voltage of capacitive MEMS and also to intensify their softening behavior. Vu et.al [37] analyzed functionally graded microbeams with a moving mass based on the Timoshenko beam theory. The beam material properties were considered to be graded in thickness by a power-law function, and they were estimated by the Mori-Tanaka scheme. Also, they used modified couple stress theory to capture the size effect. Le et.al [38] used finite element formulation to investigate Size-dependent pull-in instability of functionally graded microbeams. Based on the Von Kármán nonlinear relationship, a beam element was derived and employed to establish the discretized governing EQ for the microbeams. Results showed that the pull-in voltage was increased by the increase of the power-law exponent and the microscale parameter.

One of the best ways to improve the performance of the MEMS is optimization. There are few studies in the literature. Abo-bakr et.al [39] did multi-objective shape optimization of axially functionally graded microbeams. Taati et.al [40] optimized functionally graded material, thickness, and aspect ratio in microbeams embedded in an elastic medium. Fu et.al [41] enlarge the quality factor in microbeams by topology optimization. Gan et.al [42] did a topology optimization design using the modified couple stress theory. Abo-bakr et.al [43] did weight optimization of axially functionally graded microbeams under buckling and vibration behaviors.

As can be seen, microbeams with different models and boundary conditions are used for applications such as making sensors, so their optimal design can improve the performance of devices such as microsensors. The main goal of this research is to find the dimensions of the clamped microbeam that important functions in the performance of microsensors have their maximum values. It is also worth mentioning that one of the special applications of sensors is to detect the presence of substances such as the coronavirus, so the optimal design of such sensors, especially from a mechanical point of view, can increase their efficiency. In this study, multi-objective optimization of two-layer micro clamped-clamped microsensor, which is used to detect viruses, is done by using the genetic algorithm in Matlab. First, the microsensor is modeled as a microbeam that is clamped on both ends. Second, based on the previous studies, sensitivity, quality factor, and stress which are three important parameters of microsensors are selected as objective functions. Also, the dimensions of the microbeam are selected as design variables. In the end, results are shown based on classical and non-classical theories, and the best points are selected.

## 2- Modeling:

The microsensor is modeled as a clamped-clamped microbeam that has 2 layers. One layer is silicon and another one is quartz crystal. Quartz crystal is a piezoelectric material and has a high sensitivity. It is assumed that the microbeam is fixed on both ends and doesn't have any displacement or rotation on the boundary conditions. The model is shown in Fig. 1. The Thickness of the piezoelectric and silicon layers are $h_1$ and $h_2$ respectively. Also, the length of the microbeam

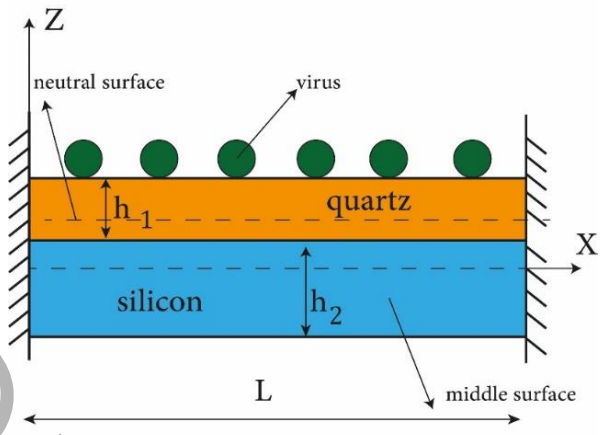


**Fig. 1. The model of the microsensor with 2 layer and clamped ends**

$L$ and width of it is $b$.

There is no external heat, and the temperature of the environment is $300K$. Viruses are external mass and when they sit on the microbeam, the total mass and the natural frequency of the system change. The mass of absorbers and electrode layer are very low so in this study, they are ignored.

There are 3 important functions: Sensitivity, Quality factor, and Maximum stress. Sensitivity and quality factors are the important functions of the microsensors [1]. In order to have high measurement quality and accuracy, the values of these functions must be high. On the other hand, for high safety and to prevent failure, maximum stress on the system must be low.

### 2- 1- Sensitivity:

The sensitivity is calculated as [1]:

$$S=\frac{\Delta f}{\Delta m}=-\frac{2f_0^{\,2}}{A\sqrt{\rho\mu}} \tag{1}$$

Where m is the mass, $\rho,\mu$ are the density and the shear modulus of the piezoelectric. $A$ is the active surface of the piezoelectric layer. In this study, all the surface of the quartz is assumed active. Also $f_0$ is:

$$f_0=\frac{\omega_0}{2\pi} \tag{2}$$

Where $\omega_0$ is the first circular natural frequency of the system. To calculate $\omega_0$ Rayleigh's method is used. Based on Rahi's investigation [15] strain and kinetic energy of the 2 layers microbeam is calculated as:

$$\pi_s=\frac{1}{2}\left\{\sum_{i=1}^{n=2}E_i\tilde{I}_i+\frac{6E_i\bar{I}_i}{(1+\nu_i)}\left(\frac{l_i}{h_i}\right)^2\right\}\int_0^L\left[\left(\frac{\partial^2 w}{\partial x^2}\right)^2\right]dx \tag{3}$$

$$K=\frac{1}{2}\int_0^L\left[\left(\sum_{i=1}^{n=2}\rho_i A_i\right)\dot{w}^2+\left(\sum_{i=1}^{n=2}\rho_i\tilde{I}_i\right)\left(\frac{\partial\dot{w}}{\partial x}\right)^2\right] \tag{4}$$

Where $w$ is the displacement. $E_i$ ,$\rho_i$ ,$A_i$ ,$h_i$ and $l_i$ are the Young's modulus, density, area, thickness, and material length scale parameters of each layer respectively. Also, $\nu_i$ is the Poisson's ratio of each layer and $\bar{I}_i$ is the moment of inertia of each layer about its neutral surface and calculated as:

$$\bar{I}_i=\frac{b_i h_i^3}{12} \tag{5}$$

where $b_i$ is the width of each layer.

Also $\tilde{I}_i$ is calculated as:

$$\tilde{I}_i=\bar{I}_i+A_i\bar{z}_{ni}^{\,2} \tag{6}$$

where $\bar{z}_{ni}$ is the distance between the neutral surface of each layer and the neutral surface of all the system and are calculated as:

$$\bar{z}_{n1}=\frac{1}{2}\left(h-2e-h_1\right)$$
$$\bar{z}_{n2}=\frac{1}{2}\left(h-2e-h_2\right)-h_1 \quad (7)$$

where $h$ is the total thickness of the microbeam and $e$ is the distance of the neutral surface of all the system from the coordinate system and calculate as:

$$e=\frac{1}{2}\frac{\left(E_2-E_1\right)\left(h_2^{\,2}-hh_2\right)}{E_1h-\left(E_2-E_1\right)h_2} \quad (8)$$

It is assumed that the system has a harmonic vibration so $w$ is defined as:

$$w\left(x,t\right)=X\left(x\right)T\left(t\right) \quad (9)$$

where

$$T\left(t\right)=e^{i\omega_0 t} \quad (10)$$

Because the microbeam is fixed on both ends, this function is proposed to satisfy the geometrical boundary conditions:

$$X=X_{max}\left(1-\cos\left(\frac{2\pi x}{L}\right)\right) \quad (11)$$

By substituting Eq. (5-10) into Eq. (3-4), the first circular natural frequency is obtained:

$$\omega_0=\left(\frac{N\left(\frac{8\pi^4}{L^3}\right)}{M\left(1.5\right)L+G\left(\frac{2\pi^2}{L}\right)}\right)^{\frac{1}{2}} \quad (12)$$

where

$$N=\left\{\sum_{i=1}^{n=2}E_i\tilde{I}_i+\frac{6E_i\bar{I}_i}{\left(1+\nu_i\right)}\left(\frac{l_i}{h_i}\right)^2\right\}$$
$$M=\left(\sum_{i=1}^{n=2}\rho_iA_i\right) \quad (13)$$
$$G=\left(\sum_{i=1}^{n=2}\rho_i\tilde{I}_i\right)$$

It should be noted that the above equations are obtained based on the modified Couple stress theory. In this theory, the amount of strain energy is obtained differently than in the classical theory. The amount of strain energy in this theory is obtained from the following relationship:

$$\pi_s=\frac{1}{2}\int_V\left(\sigma_{ij}\varepsilon_{ij}+m_{ij}\,\chi_{ij}^s\right)dV \quad ;$$
$$i=x,y,z \quad and \quad j=x,y,z \quad (14)$$

where $V$ is the volume of the system. In addition, the components of the stress tensor $\sigma_{ij}$, the strain tensor $\varepsilon_{ij}$, the deviatoric part of the symmetric couple stress tensor $m_{ij}$ and the symmetric curvature tensor $\chi_{ij}^s$ calculated as follows:

$$\sigma_{ij}=2\mu\varepsilon_{ij}+\lambda\varepsilon_{kk}\delta_{ij} \quad ; \quad m_{ij}=2\mu l^2\chi_{ij}^s \quad (15)$$

$$\varepsilon_{ij}=\frac{1}{2}\left(u_{i,j}+u_{j,i}\right) \quad ; \quad \chi_{ij}^s=\frac{1}{2}\left(\theta_{i,j}+\theta_{j,i}\right) \quad (16)$$

$$\theta_i=\frac{1}{2}\epsilon_{ijk}\,u_{k,j} \quad (17)$$

where, $\theta_{i,j}$ is the gradient of rotation, $\theta_i$ is infinitesimal rotation vector, $\in_{ijk}$ is alternating tensor (or permutation symbol), and $u_i$ is components of the displacement vector. The parameters $\left(\lambda,\mu\right)$ and $l$ are called Lamé constants and the material length scale parameter, respectively. The Lamé constants can also be written regarding Young's modulus $E$ and Poisson's ratio $\vartheta$ as follows:

$$\lambda=\frac{\vartheta E}{\left(1+\vartheta\right)\left(1-2\vartheta\right)} \quad ; \quad \mu=\frac{E}{2\left(1+\vartheta\right)} \quad (18)$$

The verification of this method is presented in Table 1. Results based on classical theory, non-classical theory, and COMSOL model are compared for single-layer and two-layer microbeam. Also, the difference between COMSOL results and the other results is calculated.

### 2- 2- Quality factor:

The quality factor of one-layer microbeam is calculated as [2]:

$$Q^{-1}=\frac{E\alpha^2T_o}{C_p}\left(\frac{6}{\xi^2}-\frac{6}{\xi^3}\frac{\sinh\left(\xi\right)+\sin\left(\xi\right)}{\cosh\left(\xi\right)+\cos\left(\xi\right)}\right) \quad (19)$$

where $E$ is the Young's modulus, $C_p$ is the heat capacity,

**Table 1. Results verification based**

| Number of layers | First natural frequency | | | | |
|---|---|---|---|---|---|
| | Classical theory | Non-classical theory (Modified couple stress theory) | COMSOL model | Difference COMSOL result with classical result | Difference COMSOL result with non-classical result |
| **Single layer** | 2.150e5 | 2.240e5 | 2.157e5 | 0.32% | 3.84% |
| **Two-layers** | 5.34e5 | 5.52e5 | 5.39e5 | 0.74% | 2.41% |

$\alpha$ is the thermal expansion coefficient, $T_o$ is the surrounding temperature, and

$$\xi = b\sqrt{\frac{\omega_0}{2\chi}} \tag{20}$$

where

$$\chi = \frac{H}{\rho C_p} \tag{21}$$

where $H$ is heat conductivity and $\rho$ is density.

In this study the microbeam is modeled as 2-layer microbeam so above values are substituted by approximated values which are the average of properties values of all layers. These values are defined as:

$$E_e = \frac{E_1 h_1 + E_2 h_2}{h_1 + h_2} \tag{22}$$

$$C_e = \frac{\sum_{i=1}^{n=2} \rho_i h_i C_i}{\sum_{i=1}^{n=2} \rho_i h_i} \tag{23}$$

$$\alpha_e = \frac{\sum_{i=1}^{n=2} \alpha_i h_i}{\sum_{i=1}^{n=2} h_i} \tag{24}$$

$$H_e = \sum_{i=1}^{n=2} \frac{H_i}{h_i} \left( \sum_{i=1}^{n} h_i \right) \tag{25}$$

$$\rho_e = \frac{\sum_{i=1}^{n=2} \rho_i h_i}{\sum_{i=1}^{n=2} h_i} \tag{26}$$

2- 3- Maximum stress:

Maximum stress is calculated as [40]:

$$\sigma_{max} = (Ez)_{max} \left( \frac{\partial^2 w}{\partial x^2} \right)_{max} \tag{27}$$

where

$$(Ez)_{max} = (E_i h_i)_{max} \tag{28}$$

According to the Eq. (8-10) for the calculation of the maximum values of $\frac{\partial^2 w}{\partial x^2}$ it is necessary that the maximum value of the $X$ calculated. It is assumed that the system is a simple mass-spring system then the maximum value of the displacement is defined as:

$$w_{max} = \frac{F}{k} \tag{29}$$

Based on Eq. (11) $k$ is calculated as:

$$k = N\left( \frac{8\pi^4}{L^3} \right) \tag{30}$$

and $F$ is the weight of the viruses which is calculated as:

$$F = (\Delta m g) \tag{31}$$

where

$$\Delta m = \left(\frac{A_B}{A_p}\right) m_p = \left(\frac{bL}{A_p}\right) m_p \tag{32}$$

where $A_B$ and $A_p$ are the area of microbeam and particles respectively. As a result, maximum stress is calculated as:

$$\sigma_{max} = C\,\sigma^* \tag{33}$$

where

$$C = \frac{g\rho_p}{A_p} \tag{34}$$

$$\sigma^* = (E_i h_i)_{max} \frac{(bL)}{N\left(\frac{8\pi^4}{L^3}\right)} \left(\frac{2\pi}{L}\right)^2 \tag{35}$$

## 3- Optimization:

Objective functions:

Three important functions of the microsensor are calculated. In the next step the optimization of the microsensor is done by choosing these functions as objective functions. Objective functions are defined as:

$$S = f_1(h_1, h_2, b, L) \tag{36}$$

$$-Q = f_2(h_1, h_2, b, L) \tag{37}$$

$$\sigma^* = f_3(h_1, h_2, b, L) \tag{38}$$

The genetic algorithm is selected for optimization. This algorithm obtains the minimum values of functions so the negative sign should be applied to the quality factor because the maximum value of the quality factor is the target of the design. Also, in Eq. (28), $C$ is a constant value, so $\sigma^*$ is selected as an objective function.

Design variables:

Dimensions of the microbeam are selected as design variables:

$$[x_1, x_2, x_3, x_4]^T = [h_1, h_2, b, L]^T \tag{39}$$

**Table 2. Bounds of design variables**

| Variable | Lower bound($10^{-6}$) | Upper bound($10^{-6}$) |
|---|---|---|
| $x(1)$ | 10 | 100 |
| $x(2)$ | 10 | 100 |
| $x(3)$ | 40 | 300 |
| $x(4)$ | 200 | 1000 |

There are some limits to make a microbeam, also equations of the microbeam are calculated based on the Euler-Bernoulli beam theory. Some constraints are set to satisfy these conditions:

$$h_1 + h_2 \le 0.1L \tag{40}$$

$$2(h_1 + h_2) \le b \tag{41}$$

$$L \ge 3b \tag{42}$$

There are lower and upper bounds for design variables that are shown in Table 2. These bounds are arbitrary.

The optimization is done by Matlab software and numerical results are shown in the next section.

## 4- The results and discussion

The results of the optimization are presented in this section. Geometrical characteristics were defined in the previous sections. The Mechanical and thermal properties of layers are described in Table 3. Results are obtained based on classical and non-classical theories. To obtain results based on classical theory, the ratio of material length scale parameters of each layer $(l_i)$ to thickness in Eq. (3) is assumed zero. The best values of functions are shown in Figs. 2 and 3 based on classical and non-classical theories.

Values are approximately equal in both Figs. In other words, the size effect doesn't have a significant effect on the optimization results. It is necessary to mention that the material length scale parameters are assumed constant and if they change according to different sizes, results may change. The targets of the design are that the sensitivity and quality factor increase while maximum stress decreases. Results show that when the maximum stress decreases and sensitivity increases, the quality factor decreases which is undesirable. Optimum values are described in Tables 4 and 5 based on

**Table 3. Properties of each layer [1, 15, 44-46]**

| Property/material | Unit | $SiO_2$(quartz) | Si |
|---|---|---|---|
| **E** | Gpa | 72.52 | 170 |
| **ν** | - | 0.166 | 0.22 |
| **μ** | Gpa | 30.97 | 69.67 |
| **ρ** | $kg/m^3$ | 2650 | 2233 |
| ***l*** | Mm | 2.4 | 1 |
| **C** | J/kg K | 700 | 812.33 |
| **H** | W/m K | 1.3 | 156 |
| **α** | $10^{-6}/K$ | 12.3 | 0.262 |

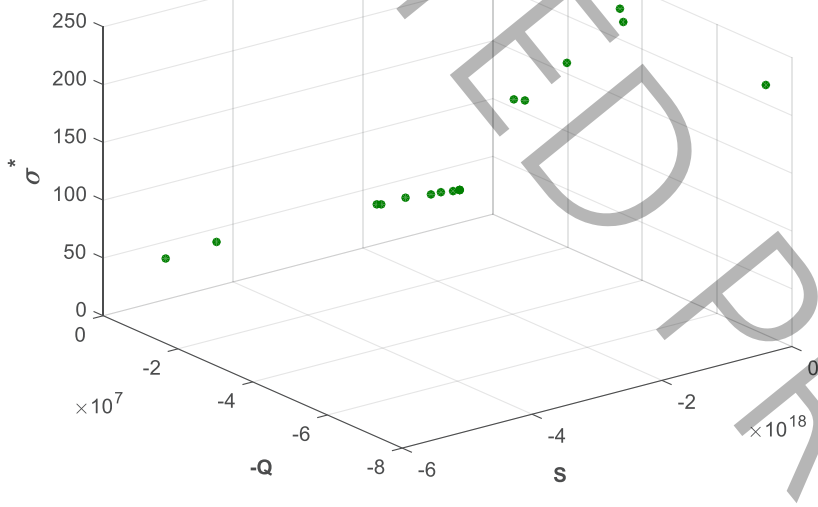


**Fig. 2. The best values based on the non-classical theory**

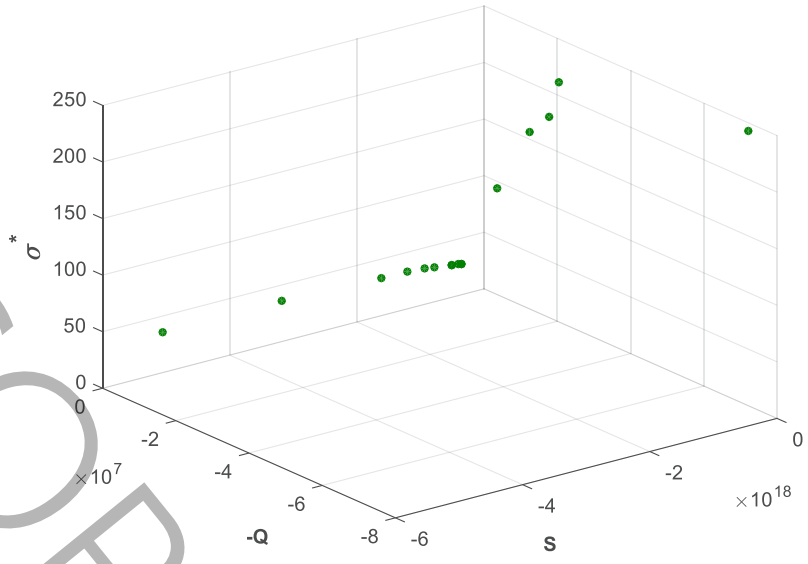


**Fig. 3. The best values based on the non-classical theory**

**Table 4. Optimum values of design variables and objective functions based on non-classical theory**

| Design variables | | | | Objective functions | | |
|---|---|---|---|---|---|---|
| $h_1(\mu m)$ | $h_2(\mu m)$ | $b(\mu m)$ | $L(\mu m)$ | S | -Q | $\sigma^*$ |
| 10.00001 | 10 | 40.00019 | 200.0001 | -5.37E+18 | -5736279 | 48.48958 |
| 10.00001 | 10.00001 | 40.00007 | 207.7847 | -4.61E+18 | -6110387 | 52.33772 |
| 10.51563 | 11.1831 | 43.4092 | 516.059 | -1.26E+17 | -inf | 282.1554 |
| 20.26477 | 10.03297 | 63.5008 | 304.1106 | -6.93E+17 | -1454709 | 32.51608 |
| 21.5693 | 10.00099 | 66.30716 | 315.7112 | -5.81E+17 | -1278532 | 30.90272 |
| 14.5928 | 10.00679 | 50.44574 | 246.6532 | -1.87E+18 | -2696743 | 39.81831 |
| 18.76926 | 10.08681 | 59.59902 | 288.857 | -8.92E+17 | -1720985 | 34.11644 |
| 10.13651 | 11.31398 | 43.23319 | 349.2757 | -6.13E+17 | -1.9E+07 | 135.0965 |
| 10.63673 | 11.74268 | 45.98299 | 470.0119 | -1.82E+17 | -7.6E+07 | 223.6882 |
| 12.24859 | 11.62389 | 48.90662 | 383.5296 | -3.78E+17 | -1.2E+07 | 122.0372 |
| 10.27186 | 11.57975 | 44.37774 | 402.2959 | -3.48E+17 | -2.6E+07 | 173.4422 |
| 10.09163 | 10.88153 | 45.09498 | 453.4306 | -1.98E+17 | -3.7E+07 | 234.6003 |
| 21.36367 | 10.11554 | 66.1933 | 316.4521 | -5.79E+17 | -1319306 | 31.66704 |
| 15.4833 | 10.06335 | 52.56166 | 259.2738 | -1.49E+18 | -2502233 | 39.50558 |
| 14.21698 | 10.04606 | 49.18312 | 245.2049 | -1.96E+18 | -3010588 | 41.17259 |
| 17.71979 | 10.07649 | 56.95586 | 278.8345 | -1.06E+18 | -1930309 | 35.52213 |
| 21.40262 | 10.15852 | 66.48856 | 315.8192 | -5.83E+17 | -1306174 | 31.42743 |
| 10.66798 | 11.73194 | 46.00252 | 470.0119 | -1.82E+17 | -3.8E+07 | 222.9055 |

**Table 5. Optimum values of design variables and objective functions based on classical theory**

| Design variables | | | | Objective functions | | |
|---|---|---|---|---|---|---|
| $h_1(\mu m)$ | $h_2(\mu m)$ | $b(\mu m)$ | $L(\mu m)$ | S | -Q | $\sigma^*$ |
| 10.00001 | 10.00001 | 40.00005 | 200.0002 | -5.37E+18 | -5511330 | 48.48959 |
| 13.61824 | 10.84357 | 49.62435 | 580.2286 | -6.65E+16 | -inf | 242.7347 |
| 21.34046 | 10.34957 | 64.84655 | 316.9401 | -5.97E+17 | -1406962 | 31.84542 |
| 23.64476 | 10.41862 | 69.87262 | 340.6774 | -4.31E+17 | -1177935 | 29.87044 |
| 10.21659 | 11.45183 | 46.25083 | 555.908 | -9.06E+16 | -inf | 335.9873 |
| 12.57673 | 10.60218 | 46.8494 | 470.574 | -1.59E+17 | -2.1E+07 | 183.401 |
| 22.67131 | 10.39453 | 68.02371 | 331.058 | -4.88E+17 | -1263060 | 30.74419 |
| 17.61935 | 10.34868 | 56.1217 | 281.1208 | -1.06E+18 | -2077547 | 36.40081 |
| 14.88545 | 10.15388 | 50.73379 | 250.3984 | -1.78E+18 | -2688111 | 39.48439 |
| 11.8323 | 10.05772 | 44.0286 | 218.9021 | -3.41E+18 | -4076588 | 44.6944 |
| 23.64328 | 10.41944 | 69.87345 | 340.6755 | -4.31E+17 | -1182053 | 29.8741 |
| 18.80375 | 10.27264 | 59.27222 | 290.7652 | -8.86E+17 | -1775854 | 34.4085 |
| 16.34789 | 10.25363 | 53.60937 | 266.7668 | -1.34E+18 | -2325974 | 37.74193 |
| 10.51382 | 10.97162 | 45.58434 | 397.5345 | -3.34E+17 | -1.8E+07 | 169.3175 |
| 13.18169 | 10.64089 | 47.96458 | 376.6941 | -3.79E+17 | -9993067 | 108.687 |
| 10.12545 | 10.58645 | 44.44293 | 437.4834 | -2.25E+17 | -2.4E+07 | 220.8515 |
| 21.33851 | 10.35104 | 64.84655 | 316.9401 | -5.97E+17 | -1407112 | 31.85131 |
| 10.53269 | 11.38965 | 46.58349 | 487.8446 | -1.50E+17 | -7.5E+07 | 248.8711 |

classical and non-classical theories. According to Eq. (13), there are some fractions that maybe are very high in special points so in some cases quality factor is inf which is due to the software approximation.

When the sensitivity is very high, dimensions are very small and approximately are equal to the lower bounds of design variables. Based on these results, to obtain high-quality factors, dimensions, especially length, must increase. In the cases where the maximum stress is small, the length of the microbeam is between cases that have a high-quality factor or high sensitivity, but the thickness of the piezoelectric layer is bigger than others.

Among the design variables, the thickness of the silicon layer has the least changes. It is lower than $2\mu m$ (approximately 20%). In other words, this variable has the least effect on the results.

The thickness of the piezoelectric layer changes about $14\mu m$ (approximately 140%). When the sensitivity is high, the piezoelectric's thickness is small and when the maximum stress is low, this variable is bigger. About the quality factors, this value in the best cases is between the two previous cases.

The width of the microbeam changes about $30\mu m$ (approximately 75%). Same as the thickness of the piezoelectric layer, when the sensitivity is high, the width is small. On the other hand, in the cases that have low maximum stress, the width is big. Also, when the quality factor is very high, the thickness is between the two above cases.

The length of the microbeam is the variables which have the most changes and have the most significant effect on the results. These variables change more than $580\mu m$ (approximately 190%) in the classical results. As other variables, in the cases that have high sensitivity, the length is the smallest. As the length increases, the quality factor increases and the sensitivity decreases. This parameter in the low maximum stress cases is between the above cases.

To define the best answers, two methods are used. By using Eq. (38) results are normalized. For each function, points that have the biggest size are converted to 1, and points that have the smallest size are converted to 0:

If points that have the minimum total size are considered

**Table 6. The best answers**

| Selection function | Theory | $h_1$ $(\mu m)$ | $h_2$ $(\mu m)$ | $b$ $(\mu m)$ | $L$ $(\mu m)$ | S | −Q | $\sigma^*$ | $\Sigma\bar{\Psi}$ |
|---|---|---|---|---|---|---|---|---|---|
| Γ | Non-classic | 10.00 | 10.00 | 40.00 | 200.00 | -5.37E+18 | -5736279 | 48.48958 | -0.973 |
| | classic | 10.00 | 10.00 | 40.00 | 200.00 | -5.37E+18 | -5511330 | 48.48959 | -0.973 |
| Y | Non-classic | 10.09 | 10.88 | 45.09 | 453.43 | -1.98E+17 | -3.7E+07 | 234.6003 | 0.515 |
| | classic | 10.12 | 10.58 | 44.44 | 437.48 | -2.25E+17 | -2.4E+07 | 220.8515 | 0.544 |

the best answers, Eq. (37) must use:

$$\Gamma = Min\left(-\bar{S} - \bar{Q} + \overline{\sigma^*}\right) \quad (43)$$

And if points that are approximately middle are considered the best answers, Eq. (38) must use:

$$\mathrm{Y} = Max\left(-\bar{S} - \bar{Q} + \overline{\sigma^*}\right) \quad (44)$$

Based on Eq. (39-40), the best answers are shown in Table 6.

It is obvious that by using $\tilde{\mathrm{A}}$ the best answers are obtained at the beginning of the results' interval. When $\tilde{\mathrm{O}}$ are used, lengths and widths have more changes than the thickness of layers. Also, based on classic theory, the thickness of the piezoelectric is bigger, but other variables are smaller.

## 5- Conclusion

In this study, the optimization of the clamped-clamped microsensor was done by using a genetic algorithm. All of the three objective functions are the important functions that describe the accuracy and safety of the system. Sensitivity was the relation between the changes of the mass and changes of the vibration frequency. The quality factor was a function that related to the quality of the measurement and maximum stress was the function that related to the maximum deflection and must be low to increase the safety of the system.

The microsensor was modeled as a two-layer microbeam which was fixed on both ends. One layer was silicon as a sublayer and another one was quartz as a piezoelectric layer. Rayleigh's method was used to calculate the natural frequency and it was used to calculate the sensitivity and the quality factor. To calculate the maximum stress, the system was assumed as a mass-spring system, and the maximum deflection was assumed equal to the static deflection.

Four geometrical dimensions, the thickness of each layer, the width of the beam, and the length of the beam, were selected as design variables. There were some constraints and bounds for these variables. The aims of this optimization were increasing the sensitivity and quality factor and also decreasing the maximum stress. The optimization was done by Matlab software and has these results:

- When the maximum stress decreases and the sensitivity increases, the quality factor decreases.
- The maximum sensitivity is obtained when the dimensions are small.
- Enlarging the sensor increases the quality factor.
- To decrease the maximum stress, the thickness of the piezoelectric must increase.
- The length of the microbeam has the most impact on the functions and has the most changes among the design variables (approximately 190%).
- The least effects were for the thickness of the silicon layer and has the least changes among the design variables (approximately 20%).
- Based on the $\tilde{\mathrm{A}}$ function, the best answers are at the beginning of the results' interval.
- Compared to results that are obtained based on the $\tilde{\mathrm{A}}$, the best points based on the $\tilde{\mathrm{O}}$ have the bigger dimensions.

As mentioned above, the purpose of this research was to find the dimensions of the microbeam so that all three objective functions can have their best values as much as

possible. According to the obtained results, reaching this goal causes the objective functions to be far from their maximum value, but all three functions are close to the initial demand. Considering that the main focus of the problem is to reach all three objective functions to their maximum values simultaneously, the optimal dimensions are obtained according to Eq. (40) and Table 5.

In the future, by considering new functions or applying piezoelectric effects in the equations, new optimal points can be found for the design of a two-layer or multi-layer microbeam.

## 6- Nomenclature

$m$ mass, kg
$E$ Young's modulus, GPa
$A$ Area, $m^2$
$h$ thickness, m
$b$ width, m
$\overline{z}$ distance between the neutral surface of each layer and the neutral surface of all the system, m
$e$ is the distance of the neutral surface of all the systems from the coordinate system
$l$ material length scale parameter, μm
$H$ thermal conductivity, W/m K
C heat capacity, J/kg K

***Greek symbols***

$\rho$ density, $kg/m^3$
$\mu$ shear modulus, GPa
$\omega$ natural frequency, radian/second
$v$ *Poaisson's ratio*
$\alpha$ the thermal expansion coefficient, *10-6/K*
$\sigma_{ij}$ stress tensor
$m_{ij}$ symmetric couple stress tensor
$\varepsilon_{ij}$ strain tensor
$\chi_{ij}^{s}$ symmetric curvature tensor
$\theta_i$ infinitesimal rotation vector
$\theta_{i,j}$ gradient of rotation
$\in_{ijk}$ alternating tensor
$u_i$ components of the displacement vector
$(\lambda,\mu)$ Lamé constants

***Subscript***

$i$ number of layers

## References

[1] F. Narita, Z. Wang, H. Kurita, Z. Li, Y. Shi, Y. Jia, C. Soutis, A review of piezoelectric and magnetostrictive biosensor materials for detection of COVID19 and other viruses, Advanced Materials, 33(1) (2021) 2005448.

[2] R. Lifshitz, M.L. Roukes, Thermoelastic damping in micro-and nanomechanical systems, Physical review B, 61(8) (2000) 5600.

[3] J. Dennis, A. Ahmed, M.M. Khir, A. Rabih, Modelling and Simulation of the Effect of Air Damping on the Frequency and Quality factor of a CMOS-MEMS Resonator, Appl. Math. Infor. Sci.(AMIS), 9 (2015) 729-737.

[4] W. Pan, H. Li, M. Wang, L. Wang, Elastothermodynamic damping modeling of three-layer Kirchhoff–Love microplate considering three-dimensional heat conduction, Applied Mathematical Modelling, 89 (2021) 1912-1931.

[5] R.D. Mindlin, H. Tiersten, Effects of couple-stresses in linear elasticity, Archive for Rational Mechanics and analysis, 11(1) (1962) 415-448.

[6] F. Yang, A. Chong, D.C.C. Lam, P. Tong, Couple stress based strain gradient theory for elasticity, International journal of solids and structures, 39(10) (2002) 2731-2743.

[7] G. Yun, K. Hwang, Y. Huang, P. Wu, A reformulation of mechanism-based strain gradient plasticity, Philosophical Magazine, 85(33-35) (2005) 4011-4029.

[8] D.C. Lam, F. Yang, A. Chong, J. Wang, P. Tong, Experiments and theory in strain gradient elasticity, Journal of the Mechanics and Physics of Solids, 51(8) (2003) 1477-1508.

[9] M.E. Gurtin, A.I. Murdoch, Surface stress in solids, International journal of Solids and Structures, 14(6) (1978) 431-440.

[10] C. Lim, G. Zhang, J. Reddy, A higher-order nonlocal elasticity and strain gradient theory and its applications in wave propagation, Journal of the Mechanics and Physics of Solids, 78 (2015) 298-313.

[11] R.D. Mindlin, N. Eshel, On first strain-gradient theories in linear elasticity, International Journal of Solids and Structures, 4(1) (1968) 109-124.

[12] S. Kong, S. Zhou, Z. Nie, K. Wang, The size-dependent natural frequency of Bernoulli–Euler micro-beams, International Journal of Engineering Science, 46(5) (2008) 427-437.

[13] S. Park, X. Gao, Bernoulli–Euler beam model based on a modified couple stress theory, Journal of Micromechanics and Microengineering, 16(11) (2006) 2355.

[14] H. Ma, X.-L. Gao, J. Reddy, A microstructure-dependent Timoshenko beam model based on a modified couple stress theory, Journal of the Mechanics and Physics of Solids, 56(12) (2008) 3379-3391.

[15] A. Rahi, Vibration analysis of multiple-layer microbeams based on the modified couple stress theory: analytical approach, Archive of Applied Mechanics, 91(1) (2021) 23-32.

[16] E. Loghman, F. Bakhtiari-Nejad, A. Kamali, M. Abbaszadeh, M. Amabili, Nonlinear vibration of fractional viscoelastic micro-beams, International Journal of Non-Linear Mechanics, 137 (2021) 103811.

[17] S.A. Eftekhari, D. Toghraie, Vibration and dynamic analysis of a cantilever sandwich microbeam integrated with piezoelectric layers based on strain gradient theory and surface effects, Applied Mathematics and Computation, 419 (2022) 126867.

[18] N. Ding, X. Xu, Z. Zheng, E. Li, Size-dependent nonlinear dynamics of a microbeam based on the modified couple stress theory, Acta Mechanica, 228 (2017) 3561-3579.

[19] B. Akgöz, Ö. Civalek, Analysis of micro-sized beams for various boundary conditions based on the strain gradient elasticity theory, Archive of Applied Mechanics, 82 (2012) 423-443.

[20] R. Littrell, K. Grosh, Modeling and characterization of cantilever-based MEMS piezoelectric sensors and actuators, Journal of Microelectromechanical Systems, 21(2) (2012) 406-413.

[21] H. Farokhi, M.H. Ghayesh, Size-dependent parametric dynamics of imperfect microbeams, International Journal of Engineering Science, 99 (2016) 39-55.

[22] R. Ansari, M. Ashrafi, S. Hosseinzadeh, Vibration characteristics of piezoelectric microbeams based on the modified couple stress theory, Shock and Vibration, 2014 (2014).

[23] B. Akgöz, Ö. Civalek, A size-dependent shear deformation beam model based on the strain gradient elasticity theory, International Journal of Engineering Science, 70 (2013) 1-14.

[24] A. Talimian, P. Béda, Dynamic stability of a size-dependent micro-beam, European Journal of Mechanics-A/Solids, 72 (2018) 245-251.

[25] B. Zhao, T. Liu, J. Chen, X. Peng, Z. Song, A new Bernoulli–Euler beam model based on modified gradient elasticity, Archive of Applied Mechanics, 89(2) (2019) 277-289.

[26] S. Yin, Y. Deng, T. Yu, S. Gu, G. Zhang, Isogeometric analysis for non-classical Bernoulli-Euler beam model incorporating microstructure and surface energy effects, Applied Mathematical Modelling, 89 (2021) 470-485.

[27] I. Esen, Dynamics of size-dependant Timoshenko micro beams subjected to moving loads, International Journal of Mechanical Sciences, 175 (2020) 105501.

[28] L. Chen, Y. Liu, S. Zhou, B. Wang, The reformulated micro-beam models by incorporating the general strain gradient elasticity theory (GSGET), Applied Mathematical Modelling, 90 (2021) 448-465.

[29] J. Reddy, Microstructure-dependent couple stress theories of functionally graded beams, Journal of the Mechanics and Physics of Solids, 59(11) (2011) 2382-2399.

[30] M. Kahrobaiyan, M. Rahaeifard, S. Tajalli, M. Ahmadian, A strain gradient functionally graded Euler–Bernoulli beam formulation, International Journal of Engineering Science, 52 (2012) 65-76.

[31] M.H. Ghayesh, Dynamics of functionally graded viscoelastic microbeams, International Journal of Engineering Science, 124 (2018) 115-131.

[32] J. Kim, K.K. Żur, J.N. Reddy, Bending, free vibration, and buckling of modified couples stress-based functionally graded porous micro-plates, Composite Structures, 209 (2019) 879-888.

[33] M. Kumar, B. Mukherjee, S. Sen, Analysis of static charge induced pull-in of an electrostatic MEMS, Communications in Nonlinear Science and Numerical Simulation, 96 (2021) 105690.

[34] S. Veena, A. Sthuti, H. Suresh, M. Nagaraj, Simulation and analysis of suspension based single axis mems capacitive accelerometer, International Journal of Basic and Applied Science, 11(3) (2022) 107-116.

[35] K.S. Pakhare, P. Punith, P. Guruprasad, R.P. Shimpi, On Effects of Shear Deformation on the Static Pull-in Instability Behaviour of Narrow Rectangular Timoshenko Microbeams, in: ASPS Conference Proceedings, 2022, pp. 1817-1822.

[36] S. Valizadeh, M. Fathalilou, G. Rezazadeh, Material dielectricity effects on the performance of capacitive micro-devices: a nonlinear study, International Journal of Mechanics and Materials in Design, 19(3) (2023) 537-552.

[37] A.N.T. Vu, V.N. Pham, D.K. Nguyen, Vibration analysis of functionally graded microbeams with a moving mass based on Timoshenko beam theory, in: IOP Conference Series: Materials Science and Engineering, IOP Publishing, 2023, pp. 012002.

[38] C.I. Le, V.N. Pham, D.K. Nguyen, Size dependent pull-in instability of functionally graded microbeams using a finite element formulation, in: IOP Conference Series: Materials Science and Engineering, IOP Publishing, 2023, pp. 012028.

[39] H. Abo-Bakr, R. Abo-Bakr, S. Mohamed, M. Eltaher, Multi-objective shape optimization for axially functionally graded microbeams, Composite Structures, 258 (2021) 113370.

[40] E. Taati, N. Sina, Multi-objective optimization of functionally graded materials, thickness and aspect ratio in micro-beams embedded in an elastic medium, Structural and Multidisciplinary Optimization, 58 (2018) 265-285.

[41] Y. Fu, L. Li, Y. Hu, Enlarging quality factor in microbeam resonators by topology optimization, Journal of Thermal Stresses, 42(3) (2019) 341-360.

[42] N. Gan, Q. Wang, Topology optimization design related to size effect using the modified couple stress theory, Engineering Optimization, 55(1) (2023) 158-176.

[43] H. Abo-Bakr, R. Abo-Bakr, S. Mohamed, M. Eltaher, Weight optimization of axially functionally graded microbeams under buckling and vibration behaviors, Mechanics based design of structures and machines, 51(1) (2023) 213-234.

[44] C.J. Glassbrenner, G.A. Slack, Thermal conductivity of silicon and germanium from 3 K to the melting point, Physical review, 134(4A) (1964) A1058.

[45] R. Hull, Inspec, Properties of crystalline silicon, INSPEC, the Institution of Electrical Engineers, London,

1999.

[46] A.A. Tatarinova, A.S. Doroshkevich, O.Y. Ivanshina, O.S. Pestov, M. Balasoiu, P.P. Gladyshev, Development of Siloxane Coating with Oxide Fillers for Kesteritic (CZTS) Photovoltaic Systems, Energies, 14(8) (2021) 2142.

**HOW TO CITE THIS ARTICLE**
*M. R. Davoodi Yekta, A. Rahi, Design of two layer clamped-clamped microsensor based on classical and non-classical theories, AUT J. Mech Eng., 9(1) (2025) 19-32.*

**DOI:** 10.22060/ajme.2024.23062.6116